*H. Nayeb-Hashemi**

Effects of Mode I and Mode II Overloads on Subsequent Mode I Crack Growth in AISI 4340 steels

REFERENCE Nayeb-Hashemi, H., **Effects of Mode I and Mode II overloads on subsequent Mode I crack growth in AISI 4340 steels,** *Biaxial and Multiaxial Fatigue*, EGF 3 (Edited by M. W. Brown and K. J. Miller), 1989, Mechanical Engineering Publications, London, pp. 265–283.

ABSTRACT Understanding fatigue crack growth behaviour of components subjected to steady state Mode I crack growth and transient Mode II overload, is important, particularly in turbo-generator shafts, which are subjected to steady state cyclic bending, promoting crack growth in Mode I, together with occasional transient torques, from electric faults, which cause further crack growth in Modes II and III. In order to predict fatigue life, the effect of transient Mode II loading on subsequent Mode I crack growth must be understood. In this paper the effects of both a Mode I and a Mode II overload on subsequent Mode I crack growth, are studied on a tempered AISI 4340 steel, using three and four point bend specimens. The results show that, in contrast to Mode I overloads (where the crack was either arrested or retarded for a distance of the order of transient plastic zone sizes), a Mode II overload gives rise to crack growth acceleration (for a very short distance much smaller than the Mode II transient plastic zone size). Based on a plasticity analysis, it is suggested that the mechanism of crack growth retardation in Mode I is due to plastic stretch zones at the crack front. Such plastic stretch zones are non-existent for Mode II overloads.

Visual observation of the fracture surface indicated the presence of corrosion products (black debris) at the points of Mode I overloads and absence of it at the points of Mode II overloads. In fact, fracture surface at the points of Mode II overloads appeared smooth and shiny. Scanning electron microscopy of the fracture surface did not reveal any cavities or shear cracks at the points of Mode II overloads in this material.

Introduction

Understanding the fatigue failure of components under multiaxial loading is extremely important for improved design and new system maintenance schedules. The traditional fatigue life prediction is based on the S–N curve, which is a curve relating nominal stress or strain amplitudes to the number of cycles to failure, N_f. The curve can be obtained from constant amplitude fatigue tests on actual components or from standard ASTM specimens made of the same material. Under variable loading, using a modified Palmgren–Miner law and a specific method for counting cycles, i.e., 'rain flow counting' (1)(2), one can estimate fatigue life.

An alternative fatigue life estimation method, which is widely used in nuclear and aerospace applications, for example, is based on crack propagation. The 'defect tolerant approach', as it has been called, assumes that short cracks

* Department of Mechanical Engineering, Northeastern University, Boston, MA 02115, USA

pre-exist in components. The number of cycles required to cause the subsequent propagation of such cracks to a critical length (failure point) is a measure of fatigue life. The majority of studies on fatigue crack growth have dealt with Mode I loading in which the crack growth rate (dc/dN) is related to the alternating stress intensity factor (ΔK_I) by an expression such as

$$dc/dN = A(\Delta K_I)^m \tag{1}$$

where A and m are constants.

In service, however, most components are subjected to multiaxial loading, and an existing crack may be subjected to a combination of Modes I, II, and/or III. The mechanisms of crack growth under mixed mode loading and their dependence on the micro-structure, loading pattern, mean load, and ratios $\Delta K_I/\Delta K_{II}$, $\Delta K_I/\Delta K_{III}$ are not well understood. The assumption that the crack grows in the plane of maximum tensile stress (Mode I) may not be accurate. Recent investigation (**3**) revealed an undetected crack in a turbo-generator shaft under transient torque can grow in Modes II and III and cause catastrophic failure. The results of cyclic torsion tests on four different steels (mill-annealed AISI 4140 steel, AISI 4340, A469, and A470 steels with comparable yield strengths) showed significantly different crack growth morphologies (**4**)–(**11**). In mill-annealed AISI 4140 at high growth rates ($\cong 10^{-3}$ mm/cycle) the crack growth was predominantly by Modes II and III. However, at lower growth rates ($\cong 10^{-4}$ mm/cycle or less) when approaching threshold conditions additional Mode II branch cracks were observed. Similarly, in AISI 4340 at high growth rates, the fracture mode was a combination of Modes II and III, but at low growth rate the crack deviated to a factory roof type of fracture, indicating Mode I branch cracks and Mode I crack growth. The results of Modes II and III crack growth in A469 and A470 steels showed no branch cracking at any ΔK_{II} and ΔK_{III} values. The mechanism of crack growth at all times was Modes II and III. These results indicate that crack deviation may have been influenced by microstructure as well as stress intensity level. The crack growth rate was related to either the alternating stress intensity factor for small scale yielding (ΔK_{III}) or the plastic strain intensity, $\Delta\Gamma_{III}$, for both small and large scale plasticity in Mode III. However, in order to predict a turbine shaft life, the effect of transient Modes II and III loadings on steady state Mode I crack growth due to cyclic bending (i.e., from its weight and/or possible missalignment) must be understood. The purpose of this investigation is to compare the effect of Modes I and II overload on subsequent Mode I crack growth. The specific aspects of interest are the microstructure, mean load, and transient plastic zone sizes (due to an overload) on subsequent Mode I crack growth.

Notation

c_o	Initial notch depth
c	Crack length emanating from notch root
N	Number of cycles

dc/dN	Fatigue crack growth rate
K_I, K_{II}, K_{III}	Stress intensity factors in Modes I, II, and III
$\Delta K_I, \Delta K_{II}, \Delta K_{III}$	Alternating stress intensities in Modes I, II, and III
$\Delta\Gamma_{III}$	Alternating plastic strain intensity in Mode III
W	Specimen width
B	Specimen thickness
M	Bending moment
Q	Shear force
V_c	Electrical potential spanning a notch with a crack length c
V_o	Initial electrical potential spanning a notch with $c = c_o$
$(r_p)_I, (r_p)_{II}$	Plastic zone sizes in Modes I and II
σ_y	Yield strength
K_{cl}	Stress intensity at the point of crack opening
K_{max}	Maximum stress intensity
K_{min}	Minimum stress intensity
ΔK_{eff}	Effective stress intensity range
r	Distance from crack tip
θ	Angle of plane from crack tip
$\sigma_x, \sigma_y, \tau_{xy}$	Normal and shear stresses
ν	Poisson's ratio
E	Elastic modulus
$(\varepsilon_x)_e, (\varepsilon_y)_e, (\gamma_{xy})_e$	Normal and shear strains in an elastic field
$(\varepsilon_x)_p, (\varepsilon_y)_p, (\gamma_{xy})_p$	Normal and shear strains in a plastic field
$(\varepsilon_x)^*, (\varepsilon_y)^*, (\gamma_{xy})^*$	Normal and shear strains at an elastic/plastic boundary

Experimental procedure

Materials

Studies were performed on AISI 4340 steel which had a chemical composition (%wt) of 0.40 C, 0.78 Mn, 1.77 Ni, 0.81 Cr, 0.25 Mo, 0.26 Si, 0.007 P, 0.013 S, 0.14 Cu, remainder Fe. The specimens were austenitized at 870°C for 1.5 h, followed by vigorous oil quenching. The specimens were then divided into three groups and tempered at 200°C, 400°C, and 600°C for 1.5 h. The ambient temperature mechanical properties are shown in Table 1. The yield strength of the materials were obtained from standard ASTM tensile tests, using the 0.2 per cent offset plastic strain.

Specimens

Four point bend and three point bend specimens were used for Modes I and II crack growth studies. The specimen dimensions are depicted in Fig. 1(a). The crack growth was monitored using a d.c. electric potential technique, for which a constant stabilized direct current is passed through the testpiece and the

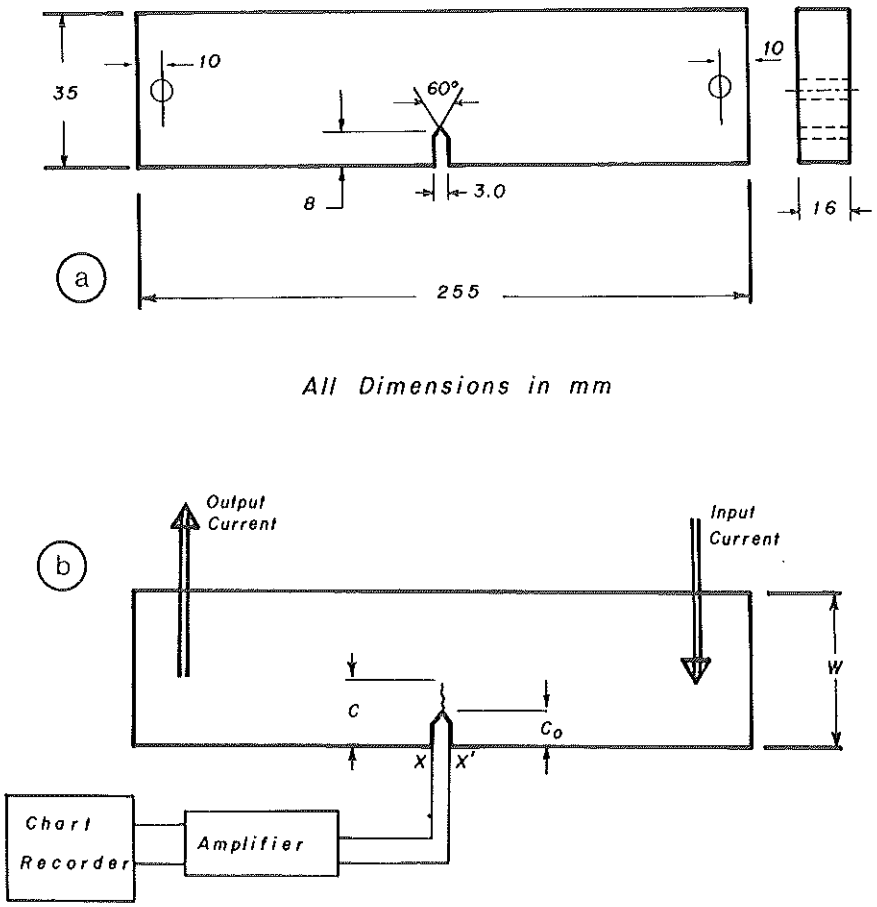

Fig 1 Schematic diagram of three and four point bending tests: (a) specimen geometry; (b) locations of current supply and potential probes

Table 1 Ambient temperature mechanical properties of AISI 4340 steel

Tempered (°C)	*Yield strength*		*Tensile strength*	
	MN/m^2	(K/in^2)	MN/m^2	(K/in^2)
200	761	(110)	967	(140)
400	640	(93)	688	(100)
600	361	(52)	426	(62)

potential changes due to increasing crack depth, measured across the notch, see Fig. 1(b). The calibration equation relating potential difference to crack length was obtained from a finite element analysis (**12**)–(**13**). This study also provided the optimum locations for probe positions. The theoretical calibration was compared with experimental results, by measuring fatigue crack lengths at the point of overloads, indicated by obvious beach markings. The results agreed well with the theoretical prediction. The relationship between crack length, c, and electrical potential across the notch, V, was found to be

$$c/w = 1.0 - 1.17513\ e^{-0.42289(V_c/V_o)} \tag{2}$$

where V_o is the initial potential corresponding to the uncracked initial notch depth c_o.

A four point symmetric loading, with respect to crack location, was chosen for crack growth studies in Mode I and an overload in Mode I. For a Mode II overload study, an unsymmetric four point bend test was used, as shown in Fig. 2. The moment and shear diagrams show that for $S_0 = 0$, the crack can be subjected to pure Mode II. An identical set-up was used by Gao *et al.* (**14**) for a mixed mode crack growth study. The fatigue crack growth rate was related to stress intensity factors in Modes I and II. For an applied moment, M, and shear force, Q, these are defined as (**14**)–(**15**).

$$K_I = \frac{6M}{BW^2}\sqrt{(\pi c)}f(c/w) \tag{3}$$

and

$$K_{II} = \frac{Q}{BW^{0.5}}g(c/w) \tag{4}$$

where B and W are the thickness and width of the specimen, respectively. Functions $f(c/w)$ and $g(c/w)$ tend to 1.122 and 0.174 as $c/w \to 0$, and 7.792 and 7.772 as $c/w \to 1$.

Fatigue tests

Modes I and II fatigue crack tests were conducted at room temperature using an MTS servo-hydraulic machine. The crack extension was continuously monitored by passing 15 A d.c. current through the specimen. The specimen was fatigue cracked at $\Delta K_I = 20\ \text{MPa}\sqrt{\text{m}}$, at stress ratios, R, of 0.05 or 0.25 and a cyclic frequency of 20 Hz. After 2 mm crack extension, ΔK_I was gradually reduced until the desired ΔK_I was reached. Tests were performed at constant ΔK_I values of 10 and 15 $\text{MPa}\sqrt{\text{m}}$, and R ratios of 0.05 and 0.25. Steady state crack growth data at constant ΔK_I were obtained by continuously adjusting the load, for the next approximately 2 mm crack extension. An overload of 100 per cent in Mode I was then applied, and its effect on Mode I crack growth at

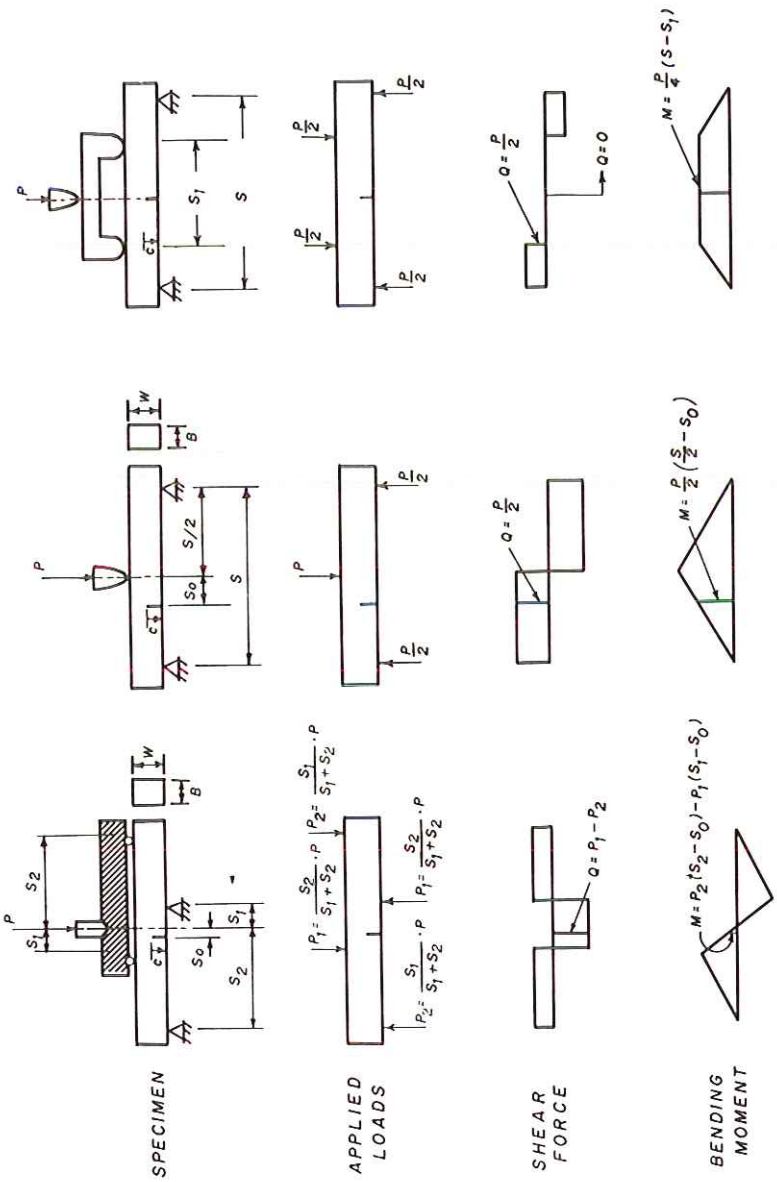

Fig 2 Bending moment and shear force diagrams for three and four point bending, showing magnitudes of shear force and bending moments for particular crack locations: after (14)

constant ΔK_I was recorded. The crack was allowed to grow beyond the induced plastic zone and, upon reaching steady state crack growth, the crack was further extended before applying a Mode II overload.

For a Mode II overload, the specimen was repositioned, so that there would not be any Mode I loading; see Fig. 2. At this position S_0, S_1, and S_2 were zero, 22.22 mm, and 73.03 mm, respectively. Force P was calculated such that the Mode II overload would result in the same transient plastic zone size as for a 100 per cent Mode I overload. The plastic zones in Modes I and II for small scale plasticity are given (see (**14**)) as

$$(r_p)_I = \frac{1}{2\pi} (K_I/\sigma_y)^2 \tag{5}$$

and

$$(r_p)_{II} = \frac{3}{2\pi} (K_{II}/\sigma_y)^2 \tag{6}$$

The same procedure was used for a 200 per cent Mode I overload and an equivalent Mode II overload. The specimen after each Mode II overload was repositioned to four point symmetric bending, and the crack was grown at constant ΔK_I for a length of the order of the transient plastic zone size. All Mode II overloads were applied when the crack length was 12–21 mm (notch length = 8 mm) in order to minimize friction effects between mating fracture surfaces.

Results and discussion

The effects of 100 per cent and 200 per cent Mode I overloads, and their equivalent Mode II overloads having the same transient plastic zone sizes, on Mode I fatigue crack growth rate at ΔK_I = 10, and 15 MPa$\sqrt{m}$ and R ratios (K_{min}/K_{max}) of 0.05 and 0.25, are shown in Figs 3–6. The results show that after a 100 per cent Mode I overload the crack growth was retarded, but without being arrested, for a distance of the order of transient plastic zone size (r_p = 0.121 mm–1.946 mm) in all three microstructures. However, a 200 per cent Mode I overload generally stopped the crack growth since the crack did not grow further after 2×10^6 cycles. Such results are familiar (**16**)–(**17**) and are known to be caused by plastic stretching and subsequent crack closure (**18**)–(**25**).

The Mode II results, however, show that, in contrast to a Mode I overload where the crack was either arrested or retarded for a distance of the order of transient plastic zone size, the Mode II overload never arrested the crack, but rather gave rise to an initial crack growth acceleration. These results are explained below.

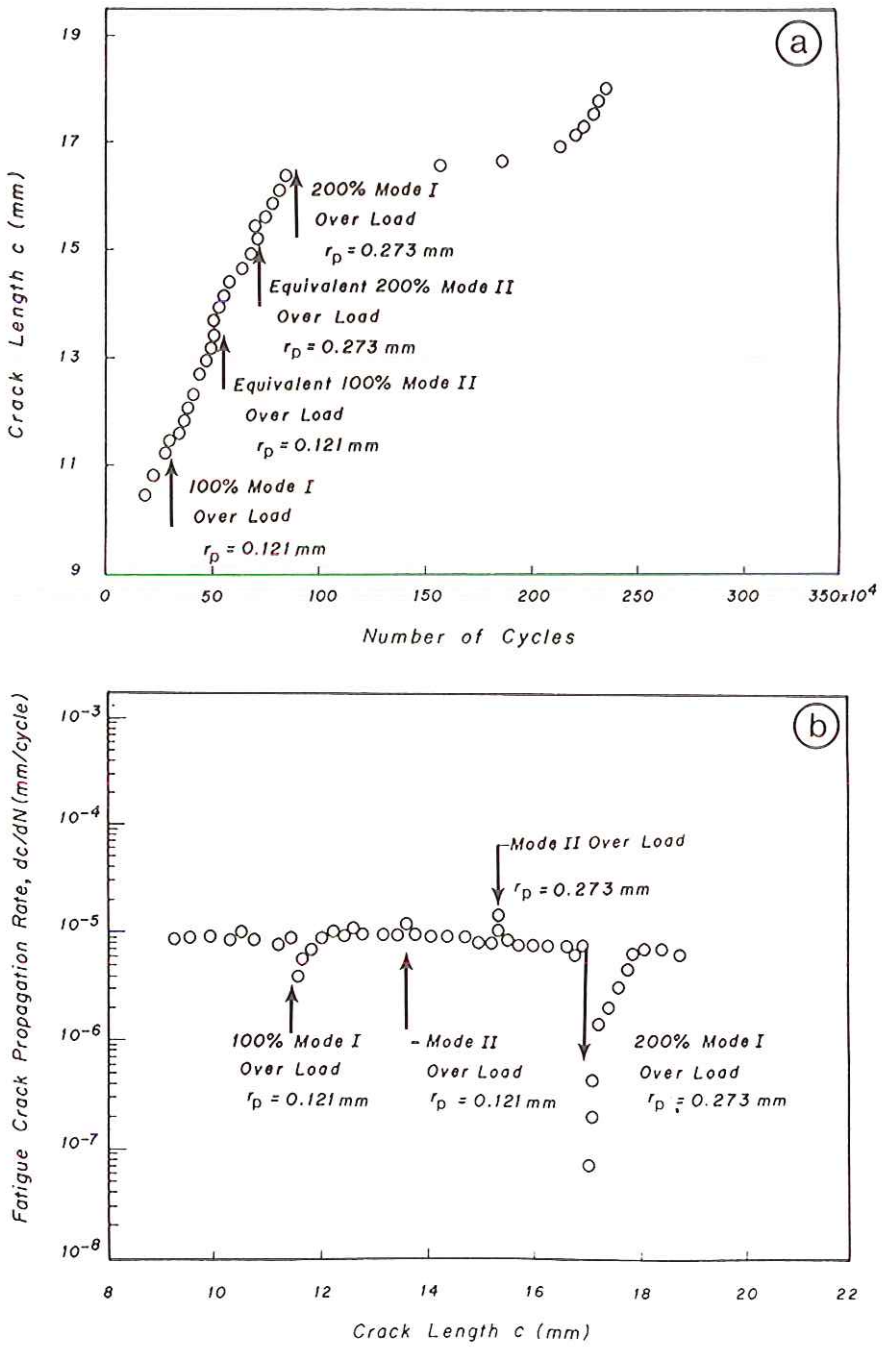

Fig 3 Effects of Mode I and Mode II overloads on Mode I crack growth rate at $\Delta K_I = 10$ MPa$\sqrt{m}$, and R Ratio = 0.05, in AISI 4340 steel tempered at 200°C ($\sigma_y = 761$ MPa): (a) crack length data; (b) crack speed data

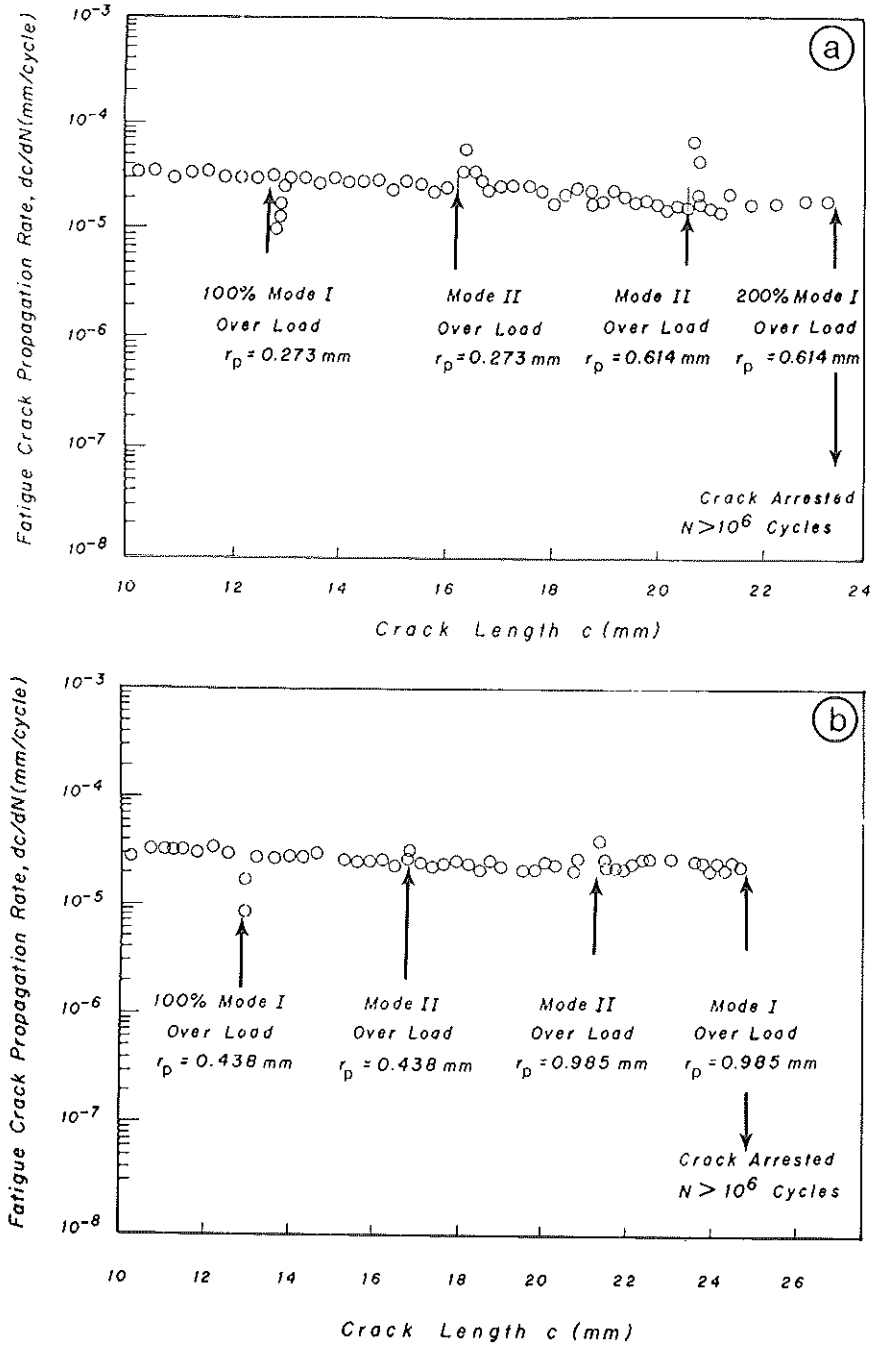

Fig 4 Effects of Mode I and Mode II overloads on Mode I crack growth rate at $\Delta K_I = 15$ MPa$\sqrt{m}$, in AISI 4340 steel tempered at 200°C ($\sigma_y = 761$ MPa): (a) $R = 0.05$; (b) $R = 0.25$

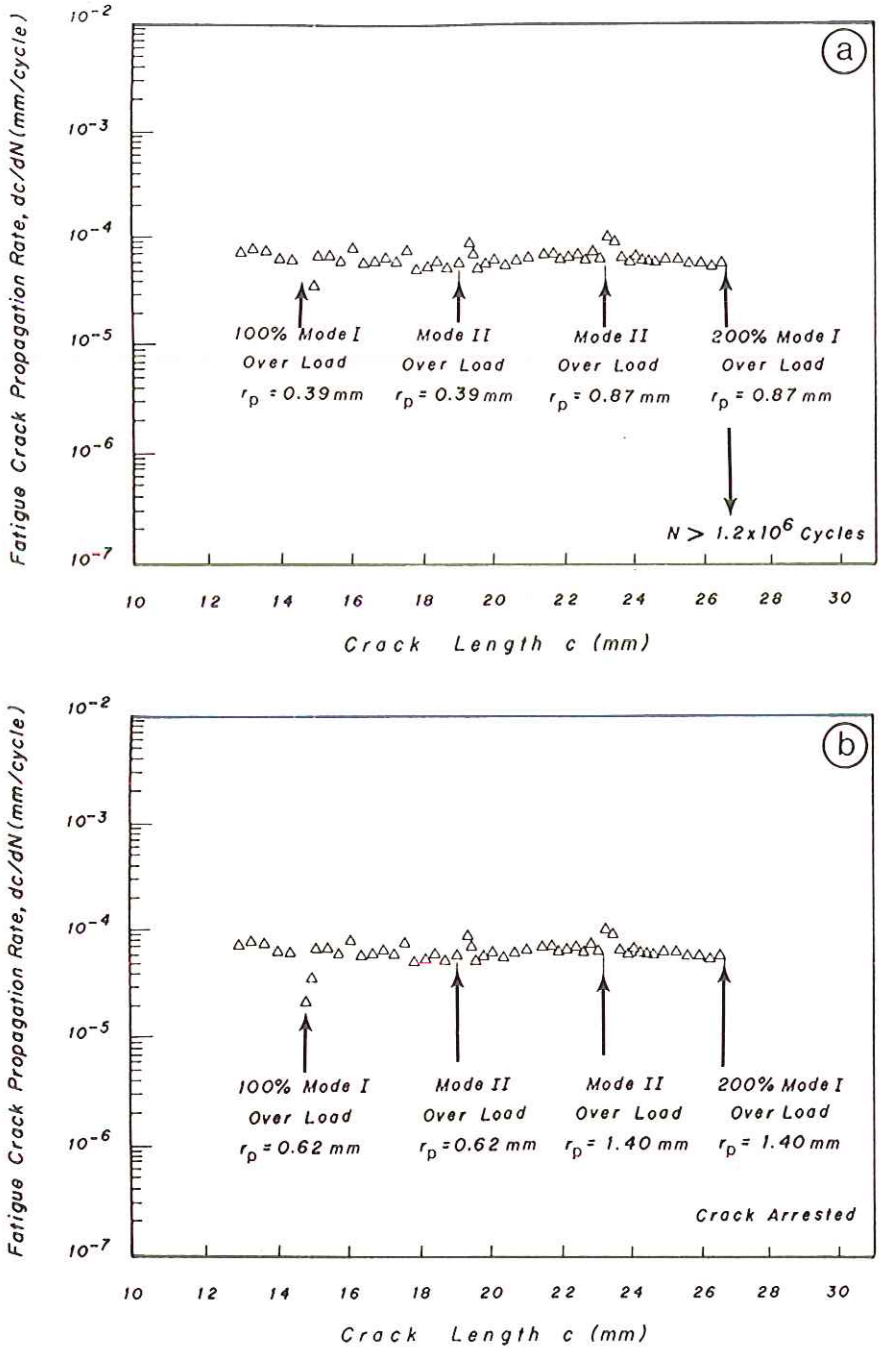

Fig 5 Effects of Mode I and Mode II overloads on Mode I crack growth rate at $\Delta K_I = 15$ MPa$\sqrt{m}$, in AISI 4340 steel tempered at 400°C ($\sigma_y = 640$ MPa): (a) $R = 0.05$; (b) $R = 0.25$

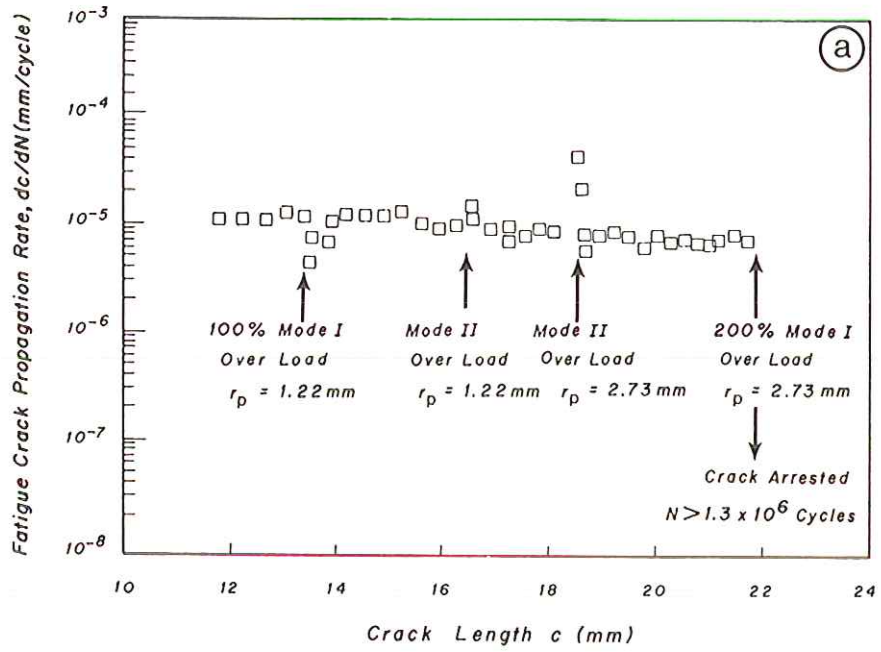

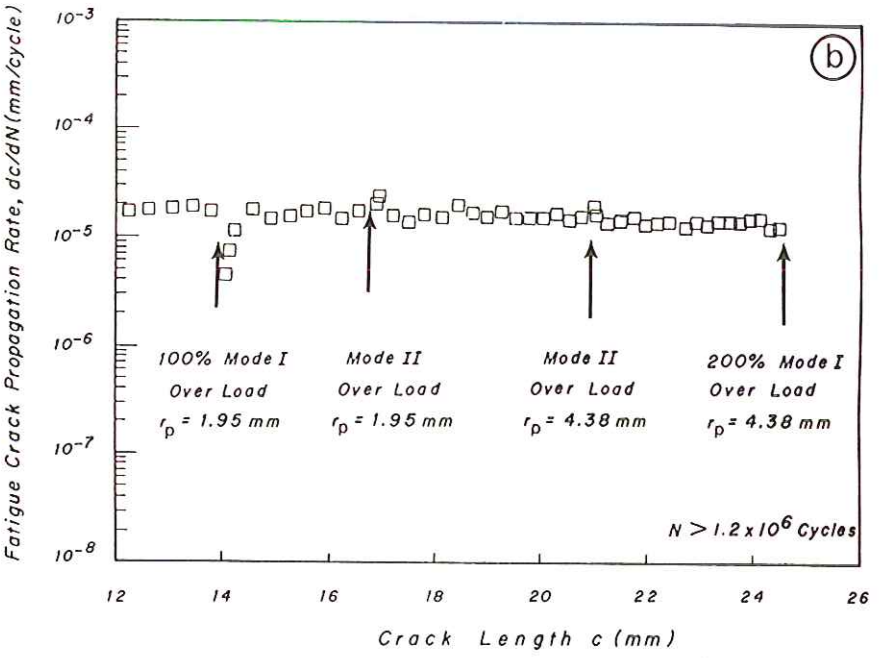

Fig 6 Effects of Mode I and Mode II overloads on Mode I crack growth rate at $\Delta K_I = 15$ MPa$\sqrt{m}$, in AISI 4340 steel tempered at 600°C ($\sigma_y = 361$ MPa): (a) $R = 0.05$; (b) $R = 0.25$

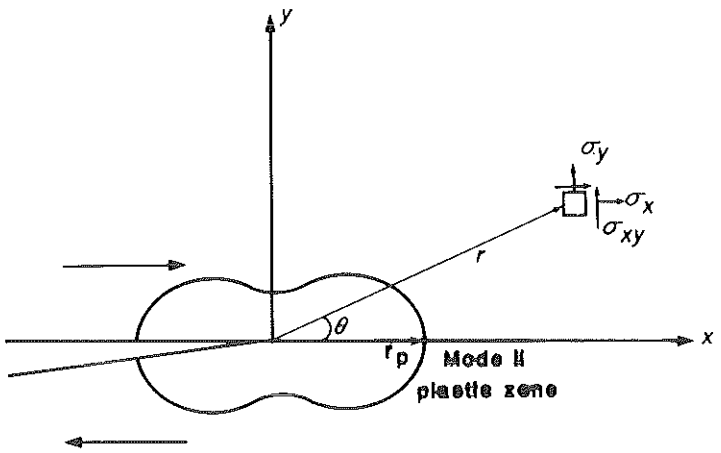

Fig 7 Schematic diagram of the plastic zone for Mode II loading

Effect of residual plastic strain

The elastic stress field (Fig. 7) for a crack subjected to Mode II loading and small scale yielding is described as

$$\sigma_x = -\frac{K_{II}}{\sqrt{(2\pi r)}} \sin\frac{\theta}{2}\left(2 + \cos\frac{\theta}{2}\cos\frac{3\theta}{2}\right) \tag{7}$$

$$\sigma_y = \frac{K_{II}}{\sqrt{(2\pi r)}} \sin\frac{\theta}{2}\cos\frac{\theta}{2}\cos\frac{3\theta}{2} \tag{8}$$

$$\tau_{xy} = \frac{K_{II}}{\sqrt{(2\pi r)}} \cos\frac{\theta}{2}\left(1 - \sin\frac{\theta}{2}\sin\frac{3\theta}{2}\right) \tag{9}$$

For plane stress conditions, the strains $(\varepsilon_x)^*$, $(\varepsilon_y)^*$, and $(\gamma_{xy})^*$, at the boundary of the elastic–plastic regime can be obtained by using Hooke's law and substituting for $r = (r_p)_{II}$ from equation (6). To avoid complexity, the plastic zone is assumed to be circular in shape, independent of θ. However, $r = (r_p)_{II}$ can be substituted as a function of θ without changing the results

$$(\varepsilon_x)^* = (\varepsilon_x)_e\Big|_{r=(r_p)_{II}} = \left\{\frac{1}{E}(\sigma_x - \nu\sigma_y)\right\}\Big|_{r=(r_p)_{II}}$$

$$= -\frac{\sqrt{3}}{3}\frac{\sigma_y}{E}\left\{\sin\frac{\theta}{2}\left(2 + \cos\frac{\theta}{2}\cos\frac{3\theta}{2}\right) + \nu\left(\sin\frac{\theta}{2}\cos\frac{\theta}{2}\cos\frac{3\theta}{2}\right)\right\} \tag{10}$$

$$(\varepsilon_y)^* = (\varepsilon_y)_e\Big|_{r=(r_p)_{II}} = \frac{1}{E}(\sigma_y - \nu\sigma_x)\Big|_{r=(r_p)_{II}}$$

$$= \frac{\sqrt{3}}{3}\frac{\sigma_y}{E}\left\{\sin\frac{\theta}{2}\cos\frac{\theta}{2}\cos\frac{3\theta}{2} + \nu\sin\frac{\theta}{2}\left(2 + \cos\frac{\theta}{2}\cos\frac{3\theta}{2}\right)\right\} \tag{11}$$

$$(\gamma_{xy})^* = (\gamma_{xy})_e\Big|_{r=(r_p)_{II}} = \frac{2\sqrt{3}}{3}(1+\nu)\frac{\sigma_y}{E}\cos\frac{\theta}{2}\left(1-\sin\frac{\theta}{2}\sin\frac{3\theta}{2}\right) \quad (12)$$

The plastic strains $(\varepsilon_x)_p$, $(\varepsilon_y)_p$, $(\gamma_{xy})_p$ inside the plastic zone, can be approximated in the following forms

$$(\varepsilon_x)_p\Big|_{0<r\leq(r_p)_{II}} = \frac{(r_p)_{II}}{r}(\varepsilon_x)^* \quad (13)$$

$$(\varepsilon_y)_p\Big|_{0<r\leq(r_p)_{II}} = \frac{(r_p)_{II}}{r}(\varepsilon_y)^* \quad (14)$$

$$(\gamma_{xy})_p\Big|_{0<r\leq(r_p)_{II}} = \frac{(r_p)_{II}}{r}(\gamma_{xy})^* \quad (15)$$

Substituting for $(\varepsilon_x)^*$, $(\varepsilon_y)^*$, and $(\gamma_{xy})^*$ from equations (10)–(12), into equations (13)–(15), the plastic strains are

$$(\varepsilon_x)_p\Big|_{0<r\leq(r_p)_{II}} = -\frac{\sqrt{3}}{3}\frac{\sigma_y}{E}\left\{\sin\frac{\theta}{2}\left(2+\cos\frac{\theta}{2}\cos\frac{3\theta}{2}\right) + \nu\left(\sin\frac{\theta}{2}\cos\frac{\theta}{2}\cos\frac{3\theta}{2}\right)\right\}\frac{(r_p)_{II}}{r} \quad (16)$$

$$(\varepsilon_y)_p\Big|_{0<r\leq(r_p)_{II}} = \frac{\sqrt{3}}{3}\frac{\sigma_y}{E}\left\{\sin\frac{\theta}{2}\cos\frac{\theta}{2}\cos\frac{3\theta}{2} + \nu\sin\frac{\theta}{2}\left(2+\cos\frac{\theta}{2}\cos\frac{3\theta}{2}\right)\right\}\frac{(r_p)_{II}}{r} \quad (17)$$

$$(\gamma_{xy})_p\Big|_{0<r\leq(r_p)_{II}} = \frac{2\sqrt{3}}{3}(1+\nu)\frac{\sigma_y}{E}\cos\frac{\theta}{2}\left(1-\sin\frac{\theta}{2}\sin\frac{3\theta}{2}\right)\frac{(r_p)_{II}}{r} \quad (18)$$

The above simplifications are similar to those suggested by McClintock for the plastic strain distribution in Mode III (**26**). Similar analyses can be performed for Mode I, and residual plastic stretch zones can be compared for Modes I and II; see Table 2. The results show that there is indeed stretching of the material ahead of the crack in Mode II, but these stretches are much smaller for Mode II than Mode I. Furthermore, the material in the crack plane ($\theta = 0$, and ahead of the crack) has zero stretch in the y direction, in contrast to Mode I which is characterized by significant stretches in the crack plane. On the other hand, the material behind the crack tip shows significant stretch in the y direction in Mode II, with very little stretch in Mode I. The results appear to confirm the Budiansky model (**18**), which describes closure as due to the residual plastic strain (stretch) in the y direction in front of the crack. Such residual stretches are missing for a Mode II overload. The results indicate that the residual plastic strain behind the crack tip from an overload may have little effect on closure in plane-stress crack growth. The results also suggest that closure may depend very little on the plastic zone shape. Indeed Mode I crack growth rate in a

Table 2 Data on residual plastic strain in Modes I and II. The residual plastic strain is given by $(\epsilon_p)_j(r/r_p)_i(E/\sigma_y)$, where $j = x, y,$ or xy, and i = I (for Mode I) or II (for Mode II), for elements of material located at a distance r and an angle θ from the crack tip and the crack plane, respectively

	Mode I			*Mode II*		
θ	x	y	xy	x	y	xy
0	0.70	0.70	0.00	0.00	0.00	1.5
10	0.67	0.73	0.22	−0.16	0.09	1.46
20	0.58	0.80	0.38	−0.31	0.17	1.35
30	0.45	0.91	0.46	−0.43	0.22	1.19
40	0.30	1.02	0.42	−0.52	0.24	0.99
50	0.15	1.11	0.26	−0.56	0.22	0.81
60	0.04	1.17	0.00	−0.58	0.17	0.65
70	−0.02	1.17	−0.32	−0.57	0.11	0.55
80	−0.02	1.09	−0.64	−0.56	0.04	0.51
90	0.04	0.96	−0.92	−0.55	−0.02	0.53
100	0.13	0.77	−1.11	−0.56	−0.05	0.60
110	0.24	0.56	−1.18	−0.61	−0.06	0.68
120	0.35	0.35	−1.13	−0.68	−0.03	0.75
130	0.42	0.17	−0.96	−0.77	0.04	0.78
140	0.45	0.03	−0.73	−0.87	0.12	0.76
150	0.41	−0.05	−0.46	−0.98	0.20	0.66
160	0.32	−0.07	−0.22	−1.07	0.28	0.48
170	0.17	−0.05	−0.06	−1.13	0.33	0.26
180	0.00	0.00	0.00	−1.16	0.35	0.00

spherodized 1090 steel, following a transient Mode II overload causing a plastic zone of $(r_p)_{II} \cong 12$ mm, showed significant crack growth acceleration, with no closure; Fig. 8.

Effect of branch cracks

Recent experimental results obtained by Lankford and Davidson (**25**) and mechanistic models developed by Suresh (**27**)(**28**) have shown that post-overload crack tip blunting, crack branching, and crack closure due to fracture surface micro roughness and fretting oxidation can substantially reduce the effective driving force for crack extension, thereby retarding growth under Mode I loading conditions. A Mode II overload, however, will not blunt the crack, and any crack extension will be in the crack plane. Indeed, the fracture surface at the point of a Mode II overload appeared shiny and smooth. On the other hand, a Mode II overload leaves some residual shear stress at the crack front. These residual shear stresses may cause further crack surface roughness interactions and may give rise to crack closure in subsequent Mode I crack growth. However, the results did not show such a closure, and neither did they show significant crack growth retardation after an overload. Furthermore, such residual shear stresses may activate slip planes that are closer to the crack plane and reduce the faceted fracture surface. Figure 9 appears to show a smoother fracture surface after a Mode II overload. Finally, the roughness induced

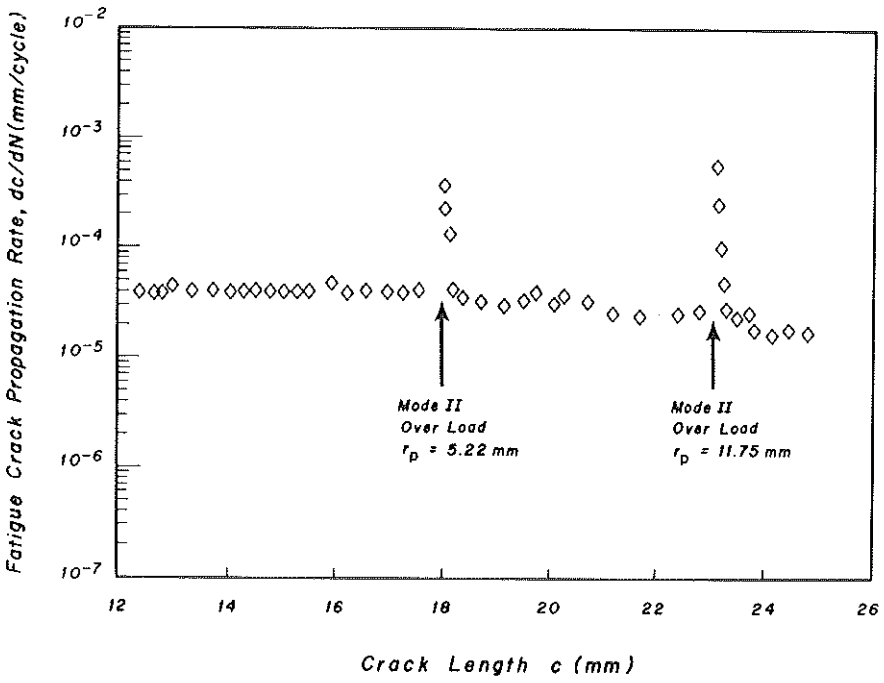

Fig 8 Effect of Mode II overloads on Mode I crack growth rate at $\Delta K_I = 25$ MPa$\sqrt{m}$, and R ratio value of 0.05, in AISI 1090 steel ($\sigma_y = 275$ MPa)

closure is mostly observed at low growth regimes, where crack extension along a single slip system can result in serrated or zig-zag fracture paths (27)(28). But at higher stress intensity values, where maximum plastic zone sizes exceed the grain size, an increasing restraint on cyclic plasticity activates more than one slip system at the crack tip leading to a more planar striation mode of crack advance by alternating or simultaneous shear (27).

Fractography

Previous Mode III fatigue crack growth studies (5)–(10) showed that the mechanism of crack growth in Mode III is by the generation and linkage of elongated cavities at the crack tip. Detailed fractography analysis using scanning electron microscopy at the point of Mode II overload did not show any such elongated cavities in AISI 4340 steels, Fig. 9. The fracture surfaces showed signs of rubbing due to Mode II overload (29). This may have even reduced the asperities and further reduced roughness induced closure. Zaiken *et al.* and Yu *et al.* (30)–(31) have shown that a compressive overload flattens the asperities close behind the crack tip, so that subsequent crack growth shows less closure, giving rise to crack growth acceleration.

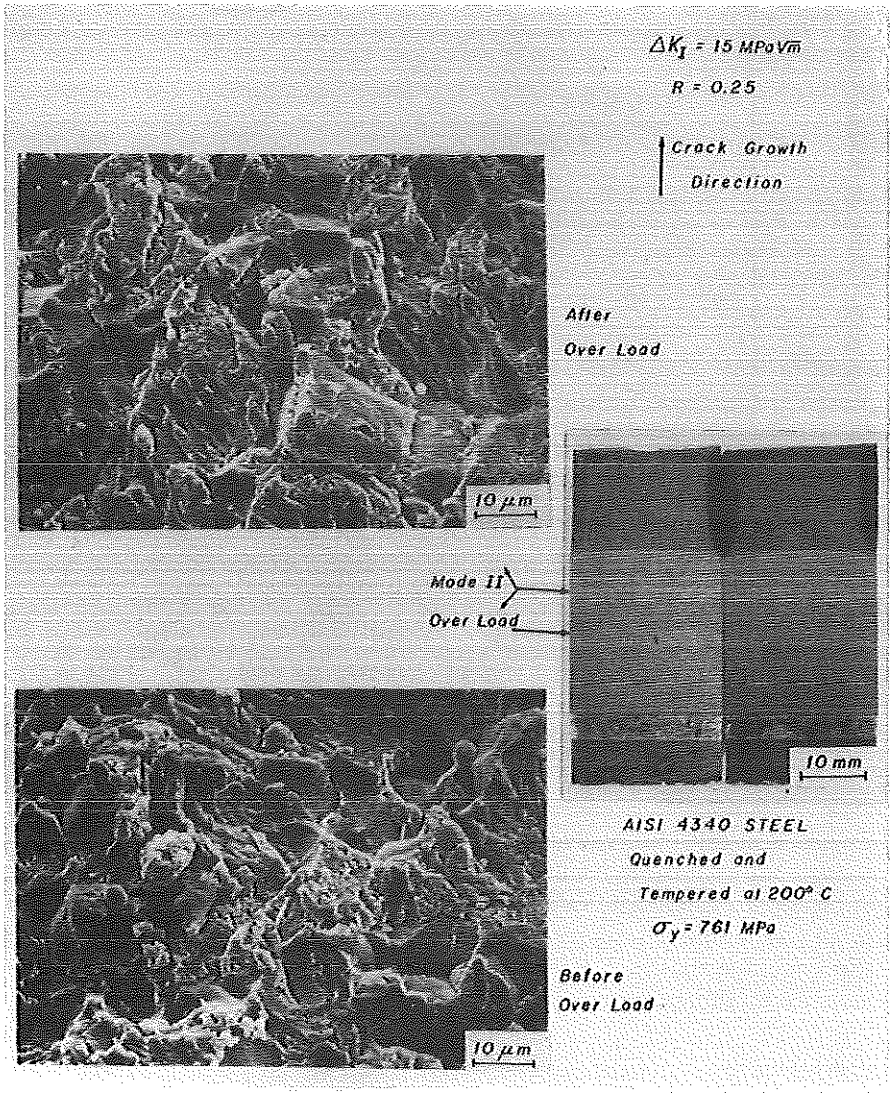

Fig 9 Micrographs of the fracture surface, in AISI 4340 steel tempered at 200°C (σ_y = 761 MPa) before and after Mode II overload, $(R_p)II$ = 0.985 mm, showing less intergranular facet after Mode II overload and shiny beach marks at the points of Mode II overloads

Visual observation of the fracture surface indicated the presence of corrosion products (black debris) at the points of Mode I overloads and absence of it for Mode II overloads. In fact the fracture surface at the points of Mode II overloads appeared smooth and shiny. A Mode II overload caused permanent crack faces displacement in 1090 steel (**29**).

Conclusions

Effects of 100 per cent and 200 per cent Mode I overloads, and equivalent Mode II overloads, on subsequent Mode I crack growth at $\Delta K_I = 10$, and 15 MPa$\sqrt{m}$, and R ratios of 0.05 and 0.25, were investigated for AISI 4340 steels. These were austenitized, quenched, and tempered at 200°C, 400°C, and 600°C. The results showed that, while a Mode I overload either arrested or retarded the crack, the Mode II overload accelerated the crack for a very short distance that was much smaller than the transient plastic zone size. Based on plastic strain analysis, it is suggested that the mechanism of crack retardation in Mode I, is due to the existence of residual plastic stretch zones at the crack front. Such residual stretch zones do not occur after a Mode II overload. Crack tip blunting and crack branching does not happen for a Mode II overload, so there is no promotion of roughness-induced closure from a Mode II overload. The residual shear stress due to a Mode II overload may activate slip planes which are closer to the crack plane, thus producing smoother and less faceted fracture surfaces.

A thick oxide layer was formed on the fracture surface at the points of Mode I overload. Such a thick oxide layer did not form at the points of Mode II overloads. The fracture surface at the points of Mode II overloads appeared smooth and shiny.

Acknowledgments

The author is indebted to Professors F. A. McClintock, Department of Mechanical Engineering, MIT, Professor J. Rossettos, Department of Mechanical Engineering, Northeastern University, and especially to Professor K. J. Miller, Department of Mechanical Engineering, University of Sheffield, UK, for valuable suggestions and encouragement. Financial support from the US National Science Foundation, Army Material and Mechanics Research Center, and the Engineering Foundation are thankfully acknowledged.

References

(1) DOWLING, N. E. (1972) Fatigue failure predictions for complicated stress–strain histories, *J. Mater.*, **7**, 71–87.
(2) SOCIE, D. F. (1977) Fatigue-life prediction using local stress–strain concepts, *Expl Mech.*, **17**, 50–56.
(3) NAYEB-HASHEMI, H. (1987) Failure modes of specimens containing surface flaws under cyclic torsion, *J. Expl Mech.*, **27**, 51–56.
(4) HURD, N. J. and IRVING, P. E. (1980) Factors influencing propagation of Mode III fatigue cracks under torsional loading, *Proc. ASTM Symp. on Design of Fatigue and Fracture Resistance Structure, ASTM STP 761*, pp. 212–233.
(5) RITCHIE, R. O., McCLINTOCK, F. A., NAYEB-HASHEMI, H., and RITTER, M. A. (1982) Mode III fatigue crack propagation in low alloy steel, *Met. Trans*, **13A**, 101–110.
(6) NAYEB-HASHEMI, H., McCLINTOCK, F. A., and RITCHIE, R. O. (1982) Effects of friction and high torques on fatigue crack propagation in Mode III, *Met. Trans*, **13A**, 2197–2205.
(7) RITCHIE, R. O., McCLINTOCK, F. A., TSCHEGGE, E. K., and NAYEB-HASHEMI,

H. (1982) Mode III fatigue crack growth under combined torsional and axial loading, *ASTM Symposium on Biaxial/Multiaxial Fatigue, ASTM STP 853*, pp. 203–227.

(8) McCLINTOCK, F. A. and RITCHIE, R. O. (1981) Modeling low cycle torsional fatigue crack growth under variable amplitude loading, *Proc. ASME Symposium Mechanics of fatigue*, Am. Soc. Mech. Eng., AMD-Vol. 47, pp. 1–9.

(9) NAYEB-HASHEMI, H. (1982) *Predicting torsionaal fatigue crack growth (Mode III) in turbo-generator shafts*, PhD thesis, Massachusetts Institute of Technology.

(10) NAYEB-HASHEMI, H., McCLINTOCK, F. A., and RITCHIE, R. O. (1983) Micro-mechanical modeling of Mode III fatigue crack growth in rotor steels, *Int. J. Fracture*, **23**, 163–185.

(11) NAYEB-HASHEMI, H., McCLINTOCK, F. A., and RITCHIE, R. O. (1983) Influence of overloads and block loading sequences on Mode III fatigue crack propagation in A469 rotor steel, *J. Engng Fracture Mech.*, **18**, 763–783.

(12) RITCHIE, R. O., GARRETT, G. G., and KNOTT, J. F. (1971) Crack growth monitoring: optimization of the electrical potential technique using analog method, *Int. J. Fracture*, **7**, 462–467.

(13) ARANSON, G. H. and RITCHIE, R. O. (1979) Optimization of the electrical potential technique for crack growth monitoring in compact test pieces using finite element analysis, *J. Testing Evaluation*, **7**, 208–215.

(14) GAO, H., BROWN, M. W., and MILLER, K. J. (1982) Mixed-mode fatigue thresholds, *Fatigue Engng Mater. Structures*, **5**, 1–17.

(15) TADA, H., PARIS, P. C., and IRWIN, G. R. (1973) *The stress intensity handbook*, Del Research Corporation, Hellertown, PA.

(16) ELBER, W. (1970) Fatigue crack closure under cyclic tensions, *Engng Fracture Mech.*, **2**, 37–45.

(17) ELBER, W. (1971) *The significance of fatigue crack closure, damage tolerance in aircraft structures, ASTM STP 486*, pp. 230–242.

(18) BUDIANSKY, B. and HUTCHINSON, J. W. (1978) Analysis of closure in fatigue crack growth, *J. Appl. Mech.*, **45**, 267–276.

(19) NEWMAN, J. C., Jr (1981) A non-linear fracture mechanics approach to the growth rate measurement, *Fatigue crack growth measurement and data analysis, ASTM, STP 738*, pp. 5–28.

(20) JAMES, M. N. and KNOTT, J. F. (1985) An assessment of crack closure and the extent of the short crack regime in QIN (HY80) steel, *Fatigue Engng Mater. Structures*, **8**, 177–1911.

(21) SURESH, S., ZAMISKI, G. F., and RITCHIE, R. O. (1981) Oxide-induced crack closure: An explanation for near-threshold corrosion fatigue behavior, *Met. Trans*, **12A**, 1435–1443.

(22) LANKFORD, J. (1983) The effect of environment on the growth of small fatigue cracks, *Fatigue Engng Mater. Structures*, **6**, 15–31.

(23) MINAKAWA, K., MATSUO, Y., and McEVILY, A. J. (1982) The influence of duplex micro-structure in steels on fatigue crack growth in the near-threshold region, *Met. Trans*, **12A**, 439–445.

(24) NAYEB-HASHEMI, H., SURESH, S., and RITCHIE, R. O. (1983) On the contrast between Mode I and Mode III fatigue crack propagation under variable amplitude loading conditions, *Mater. Sci. Engng*, **59**, L1–L5.

(25) DAVIDSON, D. L. and LANKFORD, J. (1982) *Fatigue crack tip strains in 7075-T6 by stereo imaging and their use in crack growth models, ASTM, STP 811*, pp. 371–391.

(26) McCLINTOCK, F. A., NAYEB-HASHEMI, H., RITCHIE, R. O., WU, E., and WOODS, W. T. (1984) Assessing expired fatigue life in large turbine shafts, Power system technology program, Oak Ridge National Laboratory, Oak Ridge, Tennessee 37831, Ornal/Sub/83-9062/1.

(27) SURESH, S. and RITCHIE, R. O. (1982) A geometric model for fatigue crack closure induced by fracture surface roughness, Lawrence Berkely Laboratory, Report No. LBL-13837.

(28) SURESH, S. (1985) Fatigue crack deflection and fracture surface contact: micromechanical models, *Met. Trans*, **16A**, 249–260.

(29) NAYEB-HASHEMI, H. (1985) Effects of mode II over-loads on subsequent mode I crack growth, Northeastern University, Dept. of Mech. Eng., Technical Report No. NU ME 1225.

(30) ZAIKEN, E. and RITCHIE, R. O. (1985) On the role of compression overloads in

influencing crack closure and the threshold condition for fatigue crack growth in 7150 aluminum alloy, *Engng Fracture Mech.*, **22**, 35–48.

(31) YU, M. T. and TOPPER, T. H. (1985) The effects of material strength, stress ratio, and compressive overload on the threshold behavior of a SAE 1045 steel, *J. Engng Mater. Technol.*, **107**, 125–129.